TABLE OF CONTENTS (TOC)

Electrochemistry of Gold-Silver Alloy Nanoshells

Lorenzo Russo,[1,2] Victor Puntes[1,3,4] and Arben Merkoçi*,[1,4]

[1] Catalan Institute of Nanoscience and Nanotechnology (ICN2), CSIC and BIST, Campus UAB, Bellaterra, 08193 Barcelona, Spain

[2] Universitat Autònoma de Barcelona (UAB), Campus UAB, 08193, Bellaterra, Barcelona, Spain.

[3] Vall d'Hebron Institut de Recerca (VHIR), 08035, Barcelona.

[4] Institució Catalana de Recerca i Estudis Avançats (ICREA), P. Lluís Companys 23, 08010 Barcelona, Spain.

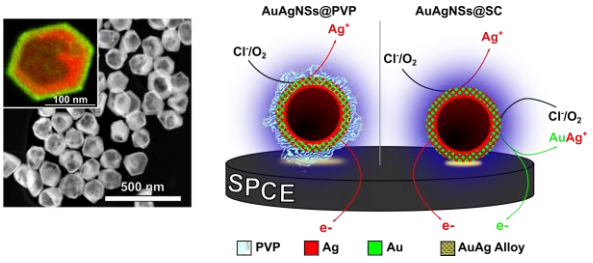

The electrochemical properties of hollow AuAg alloy nanoshells with finely tunable morphology, composition and size are studied. Through their controlled corrosion the generation of a reproducible and tunable electrochemical signal is achieved. Remarkably, the underpotential deposition of Ag^+ onto AuAg NSs surfaces is observed and its dependence on nanoparticles morphology, size and elemental composition studied, revealing a strong correlation with the relative amount of the two metals.

Arben Merkoçi, http://www.nanobiosensors.org/

Victor Puntes, http://www.inorganicnanoparticles.net/

Nano Research
DOI (automatically inserted by the publisher)
Research Article
ISSN 1998-0124
CN 11-5974/O4

Tunable electrochemistry of gold-silver alloy nanoshells.

Lorenzo Russo,[1,2] Victor Puntes[1,3,4] and Arben Merkoçi[1,4](✉)

[1] *First address, Department, University, Cit[1] Catalan Institute of Nanoscience and Nanotechnology (ICN2), CSIC and BIST, Campus UAB, Bellaterra, 08193 Barcelona, Spain*
[2] *Universitat Autònoma de Barcelona (UAB), Campus UAB, 08193, Bellaterra, Barcelona, Spain.*
[3] *Vall d'Hebron Institut de Recerca (VHIR), 08035, Barcelona.*
[4] *Institució Catalana de Recerca i Estudis Avançats (ICREA), P. Lluís Companys 23, 08010 Barcelona, Spain.*

Received: day month year
Revised: day month year
Accepted: day month year (automatically inserted by the publisher)

KEYWORDS

Au nanoshells,
nanoparticles,
surface chemistry,
underpotential deposition

ABSTRACT

The wide and growing interest in improving biosensing technologies by increasing their sensitivities and lowering their cost has led to the exploration and application of complex nanomaterials as signal transducers and enhancers. In this work, the electrochemical properties of monodispersed AuAg alloy nanoshells with finely tunable morphology, composition and size are studied in order to assess their potential as electroactive labels. The controlled corrosion of their silver content, caused by the oxidizing character of dissolved oxygen and chlorides of the electrolyte, allows the generation of a reproducible electrochemical signal easily measurable through voltammetric techniques. Remarkably, the underpotential deposition of dissolved Ag^+ catalyzed on AuAg NSs surfaces is observed and its dependence on nanoparticles morphology, size and elemental composition studied, revealing a strong correlation with the relative amount of the two metals. The highest catalytic activity is found at Au/Ag ratios higher than ≈10, showing how the synergy between both metals is necessary for triggering the enhancement of Ag^+ reduction. The ability of AuAg NSs to generate an electrocatalytic current without the need of any strong acid make of them an extremely promising material for biosensing applications.

Introduction

The rational design of advanced metallic nanoparticles (MNPs) with unique properties and functionalities has proven to be an extremely successful strategy in providing innovative and advantageous solutions to overcome the conventional intrinsic limitations of macro/micro size materials applied in *in vitro* diagnostic technologies[1]-[2], among other industrial uses. In particular, the profound understanding of the relationship between noble MNPs' localized surface plasmon resonance (LSPR) and their atomic structure, morphology and composition has led to the successful development of a number of optical biosensors, whose enhanced sensitivity and

Address correspondence to Arben Merkoçi, email: arben.merkoci@icn2.cat

flexibility outdo their more conventional predecessors.[3] In spite of that, a comparable ability in predicting and designing MNPs' electrochemical properties through their controlled synthesis hasn't been reached yet (with only few exceptions available in literature[4]), probably due to the lack of reliable and reproducible synthetic methodologies for complex nanomaterials. Interestingly though, the introduction of electroactive MNPs as signal amplification carriers or direct signal generating elements provided increased sensitivities and enhanced performances in many biosensing applications thanks to their unique redox and electrocatalytic properties,[5]·[6]·[7] which in turn emerge from their shape, surface morphology and chemical composition.[4]·[8]·[9] Indeed, electroactive MNPs represent a promising alternative to redox enzymes as electrochemical transducers since they are significantly more affordable in production and engineering, while their robustness allows easy storage (i.e. temperature, pH) and longer half-lives.[10]

Gold and silver nanoparticles (Au and Ag NPs) are probably the most widely studied and applied nanomaterials in sensing thanks to well-established understanding of their optical properties, highly susceptible to their chemical environment and easily tunable by controlling their shape, morphology and composition, as well as the electrochemical behaviour they show in certain working conditions.[11]·[12] Unfortunately, monometallic Ag NPs have found limited practical use because of a severe susceptibility to oxidation[13], resulting in a low durability and reproducibility in many bio-related applications. On the other hand, obtaining a direct electrochemical response from monometallic Au NPs requires secondary reagents or strong oxidizers able to activate catalytic effects or to generate redox active species, making extremely impractical to translate the use of this nanomaterial into electrochemical diagnostic platforms for commercial use.[8] As a result, significant effort has been put into combining Au and Ag into a single functional nanoprobe possessing both the former's high biocompatibility and stability to oxidation and the readily accessible electrochemical activity of the latter.[11]·[14] In this context, the two most explored morphologies, core shell Au@Ag NPs and AuAg alloy NPs, both exhibit an enhanced resistance to Ag oxidation thanks to an electronic density redistribution between the two noble metals, which enriches Ag orbitals with *d*-charge from Au.[15]·[16] However, no previous studies have focused on controlling the amount of this effect in order to trigger the electrochemical activity of silver without compromising the structural integrity of the system. This is in part due to the inherent immiscibility of Au and Ag at the nanoscale which, despite their perfect bulk miscibility, promotes the latter's spontaneous segregation in polycrystalline heterogeneous mixtures given its higher surface energy.[17]

Herein, hollow AuAg nanoshells (NSs) are proposed as a novel class of electroactive nanomaterial with highly promising applicability and flexibility as electrochemical labels. Their electrochemical characterization reveals the features of catalytic Ag underpotential deposition (UPD) at their surface, which has been found to depend directly on the combination of their morphology and relative chemical composition. This work provides the base for a better understanding of hollow AuAg NSs electrochemistry as well as a successful example of how the rational design of nanomaterials with controlled properties can provide suitable tools for electrochemical sensing.

Experimental Section

Silver nitrate (AgNO3), trisodium citrate (Na3C6H5O7), tannic acid (C76H52O46), HAuCl4·3H2O (99%), polyvinyl pyrrolidone (C6H9NO)n Mw ≈ 55,000 (PVP) were purchased from Sigma-Aldrich. All chemicals were used as received without further purification. Distilled water passed through a Millipore system (ϱ = 18.2 MΩ) was used in all experiments. All glassware was first rinsed with acetone and then with Millipore water before use. Buffers solutions were prepared in Milli-Q water obtained from a Millipore system Vent Filter MPK01. Both buffers, phosphate buffer (PB) and phosphate buffer saline (PBS), were prepared at

a concentration of 0.01 M and at pH7.4. PB was prepared by mixing sodium-phosphate monobasic hydrogen along with sodium-phosphate dibasic hydrogen in the desired proportion; PBS was purchased from Sigma Aldrich in tablets. Screen Printed Carbon Electrodes (SPCEs) were fabricated with a semi-automatic screen-printing machine DEK248 (DEK International, Switzerland). Electrodes were printed over Autostat HT5 polyester sheets (McDermid Autotype, UK) using Carbon Sensor Paste C2030519P4 for working (WE) and counter (CE) electrodes, Grey Dielectric Paste D2070423P5 (Gwent, The Netherlands) to insulate the contacts and define the sample interaction area, and silver/silver chloride ink for reference electrode (RE) EDAG 6037E SS (Loctite).

All nanoparticles were characterized by UV-vis spectroscopy (Perkin-Elmer "Lambda25" Spectrophotometer), Dynamic Light Scattering (DLS) Malvern Zetasizer, Transmission Electron Microscopy (TEM) and Scanning Electron Microscopy (SEM) (FEI Magellan 400L). HRTEM images were obtained using a FEI Tecnai F20 field-emission gun microscope with a 0.19 nm point-to-point resolution operated at 200 keV. The electrochemical experiments were performed by an AUTOLAB PGSTAT302N (Echo Chemie, The Netherlands) potentiostat/galvanostat which was connected to a computer and monitored by Autolab GPES software. All experiments were performed at room temperature. SCPEs were connected with the potentiostat through a homemade connector. The general protocol for the electrochemical measurements of AuAg NSs is the following: 10 μL of AuAg NSs solution (1.6x10^11 NPs/mL) were transferred into a plastic 1.5 mL Eppendorf tube containing 50 μL of a PBS 10 mM pH7.4. After incubation in the saline matrix for a given time and under stirring at 600 rpm in a thermoshaker at 25 °C, 50 μL of the mixture were dropped onto the SPCE so that to cover the three electrodes. Differential Pulsed Voltammetry (DPV) was run: after applying a fixed deposition negative potential for 60 sec, voltage was scanned between +0.6 V and +1.04 V vs RHE with 0.01 V step potential. Cyclic voltammetries (CVs) were recorded in the same conditions scanning from -0.16 V to +0.94 V vs RHE at 100 mV/sec scan rate with 0.005 V step potential.

Results and Discussion

Synthesis of Hollow AuAg Nanoshells

Hollow AuAg Nanoshells were synthetized following a protocol developed recently by our group.[18] Briefly, starting from an aqueous 5 mM polyvinyl pyrrolidone (PVP) solution containing Ag NPs of the desired size, a galvanic replacement reaction (GRR) was carried out by adding gradually a 1 mM $HAuCl_4$ solution through a syringe pump. Thanks to the difference in reduction potentials of the two noble metals (standard reduction potentials of Ag^+ and Au^{3+} are 0.7996 V and 1.498 V, respectively[19]), Au^{III} is progressively reduced onto the silver sacrificial templates surface while metallic Ag is oxidized forming a gold shell which encloses a growing inner cavity. **Figure 1 – A** shows TEM micrographs of the final stage of the reaction displaying highly monodisperse hollow AuAg NSs of c.a 60 nm in diameter, with a thin and smooth outer shell of c.a 10 nm thickness. The presence of PVP in the reaction mixture is crucial to slow down reaction kinetics and obtain thin and smooth surfaces, while at the same time provides them with increased stability towards aggregation.[20]

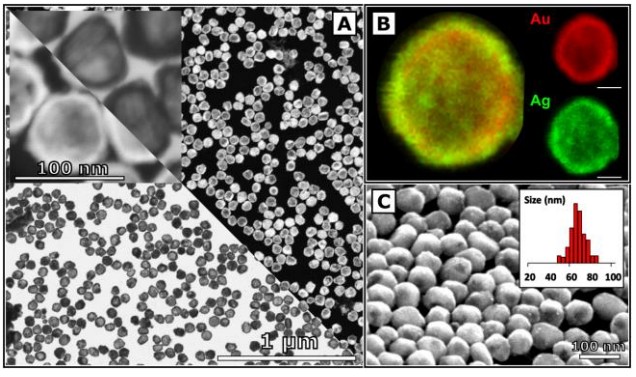

Figure 1 - A: TEM and HAADF-STEM micrographs of highly monodispersed 60.0 ± 4.4 nm AuAg NSs composed by a thin (≈10 nm) shell with a smooth surface and a large (≈40 nm) internal void. **B**: HAADF-STEM elemental distribution micrographs of a single AuAg NS (white bar corresponding to 20 nm). At the final stage of GRR Ag is found both in the Au-rich alloy outer thin shell as well as in the inner particle surface in its metallic form. **C**: SEM AuAg NSs surface characterization and size distribution.

During GRR, the difference in interdiffusion rates between the two noble metals favours the formation of a stable alloy at the interface between the particle's Ag dissolving core and the forming Au-rich shell.[21] **Figure 1 – B** shows the elemental distribution of hollow AuAg NSs by EDS mapping: while Au (*green*) is located only in the outer particle surface together with alloyed Ag (*red*), some "bulk" silver remaining from the original core is still present at the interface. Indeed, co-etchers such as HCl are needed during the hollowing process in order to vary the internal void size by corroding the "bulk", not alloyed core Ag remaining during the reaction. Thin hollow AuAg NSs with smooth integral surfaces are then obtained in high conversion yields and precisely controlled morphologies and chemical composition (**Figure 1 – C**), thanks also to the high monodispersity of the templates solution.[22]

Electrochemistry of AuAg NSs

The exposure of metallic silver to ambient atmosphere as well as nucleophilic species (such as halide anions) at pH lower than 8 is known to lead to its oxidative dissolution.[15],[23] In order to generate the electrochemical signal necessary for AuAg NSs to be used as redox reporters, the controlled corrosion of their "bulk" Ag core needs to be achieved through the use of a suitable medium.[24] Phosphate buffer saline (PBS) at pH 7.4 was therefore chosen as electrolyte not only to provide this necessary oxidizing character, given by its relatively high chlorides concentration, but also to better reproduce the typical pH and salinity of biological matrixes. **Figure 2 – A, B** show DPVs of AuAg NSs performed onto SPCEs in PBS 10 mM pH 7.5. When performing DPVs of PVP-coated AuAg NSs (**Figure 2 – A, "AuAgNSs@PVP"**), two well-defined anodic current peaks were observed: the first and more intense one (+0.8 V vs RHE, *red curve segment*), corresponding to oxidation of the metallic, "*bulk*" silver contained in the partially emptied particle core, accompanied by a weaker signal at higher oxidation potentials (+0.9 V vs RHE, *green curve segment*), given by the "*more noble*" alloyed silver. It is known that the driving force for the formation of energetically favourable alloys, such as the

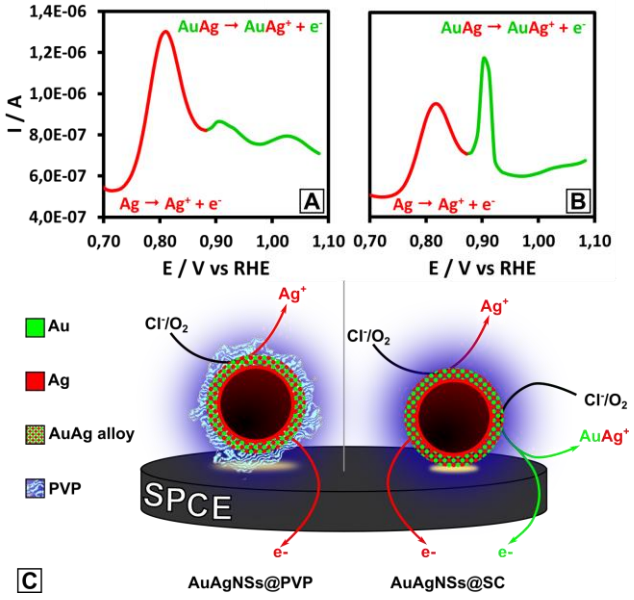

Figure 2 – A, B: DPVs in PBS 10 mM pH 7.5 of AuAg NSs coated with PVP and SC respectively. The analytical peak, found at +0.8 vs RHE, corresponds to the stripping oxidation of metallic silver, while the secondary one recorded at +0.9 vs RHE derives from the concurrent oxidation of the alloyed silver. **c**: proposed electrochemical mechanism for the AuAg NSs voltammetric profile. *Left*: PVP-coated AuAg NSs. The presence of chlorides and dissolved oxygen promotes the partial corrosion of metallic Ag from the particle's core, allowing for its detection through anodic stripping voltammetry. Only a weak signal for the oxidation of alloyed silver is observed. *Right*: SC-coated AuAg NSs. No insulating layer prevents the particle direct contact with the electrode surface, resulting in an increased current intensity in correspondence with the anodic stripping peak of alloyed silver.

gold-silver one, is the thermodynamic gain obtained by the interdiffusion of the two metals favoured by the rather small difference observed in the lattice parameters of both metals (408.53 pm for Ag and 407.82 pm for Au).[19] Compared to metallic silver, Ag atoms composing the alloy possess a higher stability towards oxidation thanks to the proximity effect[15],[16],[14], causing their characteristic anodic stripping peak to be observed at higher oxidation potentials. This behaviour is coherent with the unique electronic configuration of bimetallic AuAg systems, described also by Nishimura *et al.*, where a unique charge transfer from Au 4*f* and 5*d* levels increases electron density within Ag *d*-levels, yielding to a negative Ag oxidation state which suppresses its chemical oxidation when exposed to surrounding environments.[15],[16],[25]

description of the system is further corroborated when sodium citrate (SC)-coated hollow AuAg NSs are characterized (**Figure 2 – B, "AuAgNSs@SC"**): in this case the material does not have any polymeric coating preventing the direct contact between the thin alloy shell and the electrode surface[26] and, even if an analogous current profile is observed in term of peak potentials, their relative intensities change. In particular, the signal of the alloyed Ag, localized only in the 10 nm-thick AuAg shell, increases relevantly because of a better contact with the electrode. **Figure 2 – C** provides a schematization of the electrochemical signal's generation mechanism for AuAg NSs with each type of coatings. Moreover, the same measurement performed on a PVP-coated monometallic Ag NPs solution (**Figure S1**) shows correspondence between the $Ag^0 \rightarrow Ag^+$ oxidation peak at +0.80 - +0.82 vs RHE[23] for the three kinds of NPs studied (only sodium citrate-coated Ag NPs (**Figure S1**) cannot be measured due to their instant aggregation in PBS[27]). Interestingly, no electrochemical signal appears when using equimolar PB instead of its saline formulation (**Figure S1**). As expected, without chlorides no Ag^+ ions are generated from the particles' residual silver core for its cathodic reduction during DPV initial deposition step, and therefore no anodic stripping current can be observed, showing how crucial the presence of the corroding O_2/Cl^- solvated couple is in promoting silver oxidation. This aspect acquires notable importance since conventionally the use of metal and semiconductor NPs as electrochemical labels requires strong acids in order to generate the corresponding cations through particles corrosion.[2] The need for these impractical but necessary components precludes completely the possibility for the commercialization of such a system or their application in biological environments. Exploiting instead the mild oxidizing character of biological matrixes as the only trigger for activating the electrochemical properties of AuAg NSs represents a game-changing step forward for the development of electrochemical transducers in real-world diagnostic applications.

Au Electrocatalytic Effect

As it is widely known and reported, the elemental composition of AuAg NSs, together with their aspect-ratio (understood as the ratio between the shell thickness and the void radius), determines the localized surface plasmon resonance (LSPR) band position.[18] These two parameters depend on the extent of GRR and can be controlled by tuning the amount of Au^{III} added to the reaction mixture: depending on the stoichiometry of the process, the silver core of the particle is progressively depleted, both by the redox reaction driven by the difference in reduction potentials between the two noble metals and by the alloying process, which "extracts" metallic silver from the particle core and favours its migration towards the surface.[17] Additionally, core Ag is dissolved by the combined action of protons, dissolved oxygen and nucleophiles present in solution.[18] **Figure 3 – A** shows high magnification TEM micrographs of the different phases of the GRR, where 60 nm-sized Ag NPs are progressively converted into hollow NSs through the formation of a thin Au shell on their surface while a growing inner void is corroded from their core. During this process the relative amount of the two noble metals (Au/Ag ratio) grows accordingly: **Table 1** reports the calculated and experimental values of Au/Ag ratio, which are in good agreement with each other, for the different phases of GRR. Less reported is the effect of the nanoalloys composition on their electrochemical behaviour, explored only to our knowledge for "*bulk*" AuAg NPs[28],[29] and macroscopic AuAg micro/nano-porous electrodes.[30],[31] Thus, Cyclic Voltammetries (CVs) of AuAg NSs at different degrees of galvanic replacement conversion were carried out (**Figure 3 – B**) and revealed an increasing trend in the Ag oxidation current intensity. At the initial and intermediate stages of GRR (**Figure 3 – B**, *yellow, orange, red and purple curves*), characterized by a relatively low Au/Ag relative composition as well as a small void and an incomplete Au shell, the hollow nanocrystals display a weak anodic signal, with peak currents not overcoming the ≈ 3 μA value (**Figure 2 – B,** *inset*; **Table 1**). The higher amount of Au deposited at the later GRR stages together with the continued enlargement of the internal cavity greatly enhances the oxidation current intensity,

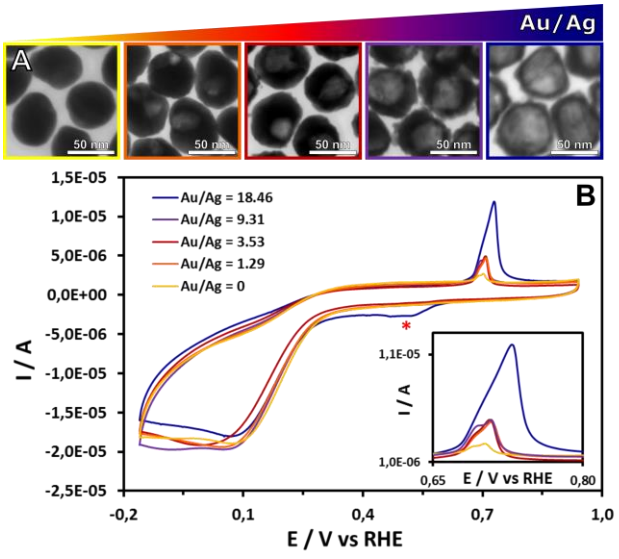

Figure 3 - A: TEM images showing the morphological evolution of silver templates during GRR. Starting from ≈ 60 nm monodispersed Ag NPs (*left*), titration with $HAuCl_4$ triggers the structural and chemical transformation leading gradually to the formation of a thin AuAg alloy shell enclosing an empty internal cavity (*right*). **B**: CVs of AuAg NSs at different GRR stages (inset showing peak currents for Ag oxidation at ≈ +0.76 vs RHE normalized over concentration). While the voltammetric profile maintains the same features in term of peaks position and shape, the current intensity increases once the GRR is started. At the latest phase, corresponding to a thin Au-rich shell enclosing a large void (*right*), the electrocatalytic $Ag^+ + e^- \rightarrow Ag^0$ reduction peak appears at +0.44 V vs RHE (*).

reaching a maximum for particles with Au-rich alloyed outer shells and large internal voids (**Figure 3 – B**, *blue curve*, **Table 1**). The reason for this electrochemical signal amplification resides probably in two synergic effects caused by the transformations in AuAg NSs morphology and chemical composition. Firstly, the increased surface-to-volume ratio obtained with the void enlargement (**Figure 3 – A**) would correspond to a higher degree of chlorides corrosion and therefore a larger amount of Ag^+ generated at the electrode surface, which in turn brings to higher oxidation currents. Secondly, when analysing the CVs of the different phases of GRR, a weak but clearly defined reduction peak appears at +0.44 vs RHE only in the case of the latest GRR stages (**Figure 3 – B**, *blue curve*): this well-known and studied feature corresponds to the UPD of Ag^+ ions onto the NSs' surface[32],[33] exploited successfully in the electrochemical silver-enhanced method with Au NPs.[34],[35],[36] The metal cations electrodeposition mechanism onto other metallic surfaces has been largely investigated at the macro-scale, while few examples of metal UPD over MNPs are found in literature.[37],[38] During the UPD process metal ions in solution can adsorb onto the MNPs surface altering the local surface charge density of the metal. Upon application of a cathodic potential the *ad*-atoms undergo a partial discharge, which corresponds to a negative partial charge transfer from the NPs excess electron density. This cathodic current is observed at reducing potentials less negative than the metal's standard reduction one. As shown by the CVs of hollow AuAg NSs bearing a Au-rich outer shell and a large internal void (**Figure 3 – B,** *blue curve*), during the cathodic scan the peak observed at -0.2 V vs Ag/AgCl represents the first deposition stage, attributed to the partial discharge of solvated Ag^+ *ad*-atoms, followed by bulk deposition of Ag only at -0.16 V vs RHE (the broad nature of the UPD peak compared to macroscale metals surfaces is attributed to AuAg NSs small sizes and faceted surface). This catalytic effect is observed only for AuAg NSs obtained at the final stages of the GRR, suggesting a correlation between morphology, surface chemical composition and the Ag UPD reaction. Indeed, variations in morphology and degree of alloying in bimetallic systems are known to influence their catalytic activity through a modulation of the electronic structure of the constituting metals.[12],[14],[39],[40] Hollow AuAg NSs at the latest GRR stages possess the highest content of Au atoms (**Table 1**), which are concentrated in the thin outer shell due to their synthesis mechanism.[18] As explained previously, the injection of Au *d*-charge

Table 1. Calculated and experimental values of Au/Ag ratio for the different phases of GRR and their corresponding anodic current. For low Au/Ag ratios, only a slight increase in peak current is observable compared with the sacrificial Ag NPs (Au/Ag = 0). At the latest stages of GRR, corresponding to the higher amount of Au deposited (Au/Ag ≈ 20), a greater signal enhancement appears.

Peak Current [μA] [a]	Au/Ag % (Theor.)	Au/Ag % (EDS)
0.66 ± 0.5	0.00	0.00
2.88 ± 0.5	1.87	1.29
2.92 ± 0.1	3.38	3.53
3.25 ± 0.2	10.77	9.31
7.76 ± 0.4	22.91	18.46

[a] Anodic current measured at +0.12 mV vs Ag/AgCl.

into Ag electronic levels results in an increased electron density localized on the particles surface.[16] Hollow AuAg NSs will therefore display higher surface potential, given its direct dependence form the metal surface excess charge[41], causing the adsorbed Ag ions to interact with a more intense generated electromagnetic field. As a consequence, Au-rich NSs will then catalyse the reduction of Ag^+ produced by PBS, generating a more intense anodic stripping current.

Following a different but agreeing description of the catalytic mechanism, hollow nanostructures are known to display better plasmonic properties than their solid counterparts thanks to the plasmon hybridization mechanism, in which the presence of cavities induce an enhancement and more homogeneous distribution of the generated electromagnetic fields.[42],[43] The adsorption and partial discharge of metal ions during the UPD, which takes place at the closest proximity to the MNPs surface, will therefore be affected by the enhanced field intensities showed by the hollowed particles, resulting in an increased Ag catalytic reduction.

We extended the study of the electronic effect on AuAg NSs electrocatalytic UPD to hollow nanoalloys of different sizes (namely 60, 80, 100, 150 nm), all having in common the final SPR maximum wavelength, found at 700 nm. As it is synthetically extremely difficult to precisely control the final relative amount of Au and Ag using templates whose silver content and total surface area vary with size at different proportionalities, fixing a common final wavelength provides a direct correlation between both the Au/Ag composition and the relative morphological aspect ratio.[18] **Figure 4 – A** shows low and high magnifications TEM dark field micrographs of 60, 80, 100, 150 nm AuAg NSs (*from top-left, clockwise*), all possessing the common hollow morphology characterized by a relatively thin outer shell and a large internal void, summarized in **Table 2**. EDS elemental mapping of these particles (**Figure 4 – B**) reveals that, while the topological distribution of Au (*green*) and Ag (*red*) is analogous among all the different sizes, their relative amount differs from size to size. Calculated and experimental Au/Ag ratios for all sizes, reported with significantly good agreement in **Table 2**, show how bigger hollow AuAg NCs

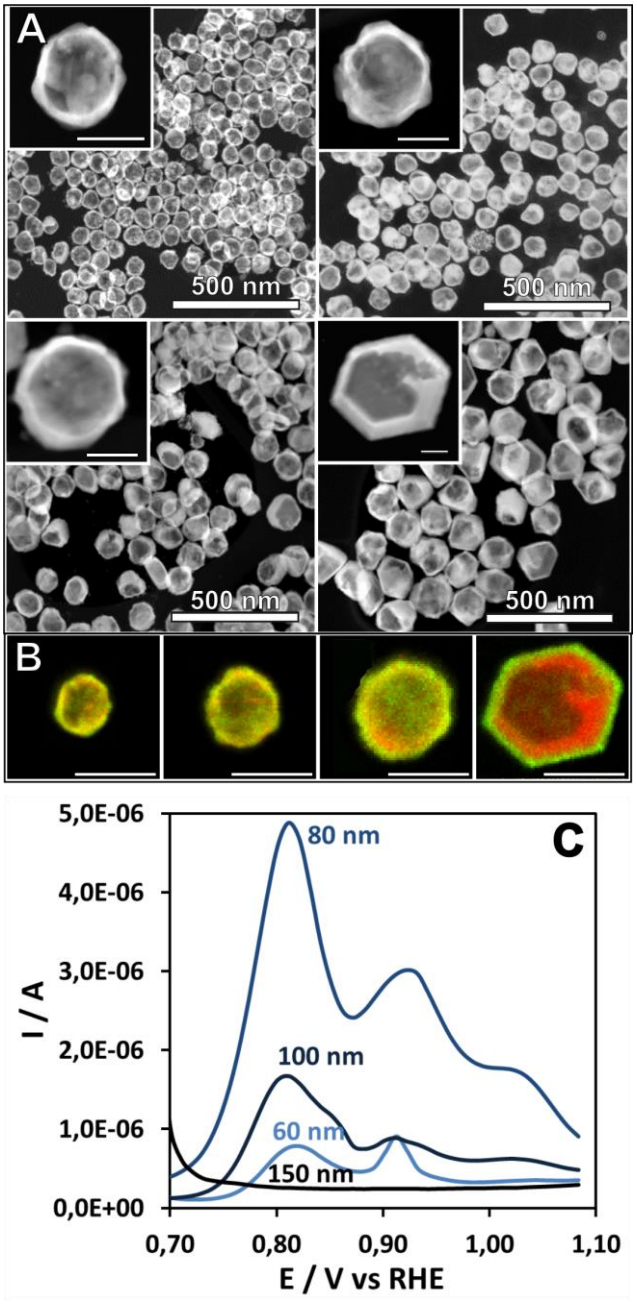

Figure 4. Scheme **A:** Dark field TEM micrographs and HRTEM images (insets) of highly monodispersed AuAg NSs of different sizes (*form top-left, clockwise*: 60, 80, 100, 150 nm). **B**: HAADF-STEM elemental distribution micrographs of individual AuAg NSs (white bar corresponds to 100 nm). **C**: DPVs of AuAg NSs of different sizes (60, 80, 100, and 150 nm): depending on the chemical composition and morphological structure different electrochemical profiles are displayed.

possess a higher Ag content compared to smaller ones, regardless of the quite constant aspect ratio between shell thickness and void size. As shown in **Figure 4 – C**, DPVs of AuAg NSs of different sizes show large current intensity variations depending on their relative noble metal content. The most intense oxidation current is observed for 80 nm-sized NSs which seem to provide the higher signal enhancement. Both 60 nm and 100 nm AuAg NSs display a lower current amplification while for 150 nm hollow nanocrystals no peak appears. By comparing these results with the Au/Ag content of each case (**Table 2**) it is clearly visible how 80 nm-sized AuAg NSs possess a high-enough Au content to trigger the electrocatalytic silver reduction through the mechanism described above. In contrast bigger particles do not possess such high-enough Au content since their alloy composition is still too rich in silver (an effect that cannot be explained by the morphological aspect ratio alone). Interestingly, even though 60 nm particles possess a sufficient Au/Ag ratio for triggering the catalysed Ag UPD, their lower anodic current intensity is a consequence of the almost complete depletion of the core metallic silver, responsible for generating the actual electrochemical signal.

Table 2. Au/Ag ratio calculated and measured by EDS, morphological features and aspect ratio of AuAg NSs of different sizes (60, 80, 100, 150 nm): a gold-rich alloy shell, together with a low aspect ratio, are necessary in order to obtain a strong oxidation signal.

Size [nm]	**60**	**80**	**100**	**150**
Au/Ag % (Theor.)	18.46	17.17	16.73	9.74
Au/Ag% (EDS)	22.91 ± 0.20	18.96 ± 0.20	14.14 ± 0.13	10.13 ± 0.12
Void size (nm)	41.6 ± 5.4	63.8 ± 7.5	68.2 ± 9.3	98.9 ± 16.5
Shell thick. (nm)	9.1 ± 1.6	12.4 ± 2.6	16.1 ± 5.2	24.1 ± 8.8
Aspect ratio[a]	**0.1** ± 0.0	**0.2** ± 0.1	**0.2** ± 0.1	**0.3** ± 0.1

[a] Aspect ratio calculated as (D-d)/d, being D the outer and d the inner diameter respectively.

Conclusions

Hollow AuAg (NSs) are presented as promising electroactive nanomaterials showing high potential and flexibility for future use as electrochemical labels for diagnostics (biosensing), beside other applications. The AuAg surface-catalysed Ag underpotential deposition is discovered and its mechanism described in detail. Thanks to it, DPV anodic oxidation signals are enhanced up to almost one order of magnitude compared to Ag NPs, depending on AuAg NSs morphology and relative chemical composition. This behaviour, previously unreported for AuAg NSs, is likely connected to the increase in surface charge density obtained with the Au enrichment of the outer shell, which seems to favour Ag^+ UPD onto it. A precise modulation of this electrocatalytic effect can be obtained by carefully design and control of the synthesis of these advanced materials, allowing the construction of efficient and robust electrochemical transducers ready for substituting enzymes in electrochemical diagnostic technologies beside other uses. This approach could be extended to other types of multimetallic nanomaterials whose diverse and selective electrocatalytic properties could be exploited as labels in immuno- and in enzymatic assays.

Acknowledgements

This work was carried out within the "Doctorat en Quìmica" PhD programme of Universitat Autònoma de Barcelona, supported by the Spanish MINECO (MAT2015-70725-R) and from the Catalan Agència de Gestió d'Ajuts Universitaris i de Recerca (AGAUR) (2017-SGR-143). Financial support from the HISENTS (685817) Project financed by the European Community under H20202 Capacities Programme is gratefully acknowledged. It was also funded by the CERCA Program/Generalitat de Catalunya. ICN2 acknowledges the support of the Spanish MINECO through the Severo Ochoa Centers of Excellence Program under Grant SEV2201320295.

Electronic Supplementary Material: Supplementary material (f **Electronic Supplementary Material**: Supplementary material (further details of the electrochemical characterization of AuAg NSs) is available in the online version of this article at http://dx.doi.org/10.1007/s12274-***-****-*.

References

[1] A. Genç, J. Patarroyo, J. Sancho-Parramon, N. G. Bastús, V. F. Puntes, J. Arbiol, Hollow metal nanostructures for enhanced plasmonics: Synthesis, local plasmonic properties and applications *Nanophotonics* **2017**, *6*, 193–213.

[2] A. Merkoçi, Nanoparticles-based strategies for DNA, protein and cell sensors *Biosens. Bioelectron.* **2010**, *26*, 1164–1177.

[3] A. Kumar, S. Kim, J. M. Nam, Plasmonically Engineered Nanoprobes for Biomedical Applications *J. Am. Chem. Soc.* **2016**, *138*, 14509–14525.

[4] H.-J. Qiu, X. Li, H.-T. Xu, H.-J. Zhang, Y. Wang, Nanoporous metal as a platform for electrochemical and optical sensing *J. Mater. Chem. C* **2014**, *2*, 9788–9799.

[5] M. M. Costa, A. de la Escosura-Muñiz, C. Nogués, L. Barrios, E. Ibáñez, A. Merkoçi, Simple monitoring of cancer cells using nanoparticles *Nano Lett.* **2012**, *12*, 4164–4171.

[6] M. Perfézou, A. Turner, A. Merkoçi, Cancer detection using nanoparticle-based sensors *Chem. Soc. Rev.* **2012**, *41*, 2606–2622.

[7] A. Merkoçi, Nanoparticles Based Electroanalysis in Diagnostics Applications *Electroanalysis* **2013**, *25*, 15–27.

[8] A. Ambrosi, A. Merkoçi, A. de la Escosura-Muñiz, Electrochemical analysis with nanoparticle-based biosystems *TrAC - Trends Anal. Chem.* **2008**, *27*, 568–584.

[9] S. O. Kelley, C. a Mirkin, D. R. Walt, R. F. Ismagilov, M. Toner, E. H. Sargent, Advancing the speed, sensitivity and accuracy of biomolecular detection using multi-length-scale engineering *Nat. Publ. Gr.* **2014**, *9*, 969–980.

[10] X. Wang, Y. Hu, H. Wei, Nanozymes in bionanotechnology: from sensing to therapeutics and beyond *Inorg. Chem. Front.* **2016**, *3*, 41–60.

[11] C. P. Byers, H. Zhang, D. F. Swearer, M. Yorulmaz, B. S. Hoener, D. Huang, A. Hoggard, W.-S. Chang, P. Mulvaney, E. Ringe, N. J. Halas, P. Nordlander, S. Link, C. F. Landes, From tunable core-shell nanoparticles to plasmonic drawbridges: Active control of nanoparticle optical properties. *Sci. Adv.* **2015**, *1*, e1500988.

[12] B. Zugic, L. Wang, C. Heine, D. N. Zakharov, B. A. J. Lechner, E. A. Stach, J. Biener, M. Salmeron, R. J. Madix, C. M. Friend, Dynamic restructuring drives catalytic activity on nanoporous gold-silver alloy catalysts *Nat. Mater.* **2017**, *16*, 558–564.

[13] Y. Zheng, J. Zeng, A. Ruditskiy, M. Liu, Y. Xia, Oxidative etching and its role in manipulating the nucleation and growth of noble-metal nanocrystals *Chem. Mater.* **2014**, *26*, 22–33.

[14] T. J. a Slater, A. Macedo, S. L. M. Schroeder, M. G. Burke, P. O'Brien, P. H. C. Camargo, S. J. Haigh, Correlating catalytic activity of Ag-Au nanoparticles with 3D compositional variations *Nano Lett.* **2014**, *14*, 1921–1926.

[15] C. Shankar, A. T. N. Dao, P. Singh, K. Higashimine, D. M. Mott, S. Maenosono, Chemical stabilization of gold coated by silver core-shell nanoparticles via electron transfer *Nanotechnology* **2012**, *23*.

[16] S. Nishimura, A. T. N. Dao, D. Mott, K. Ebitani, S. Maenosono, X-ray Absorption Near-Edge Structure and X-ray Photoelectron Spectroscopy Studies of Interfacial Charge Transfer in Gold–Silver–Gold Double-Shell Nanoparticles *J. Phys. Chem. C* **2012**, *116*, 4511–4516.

[17] E. a. Lewis, T. J. a. Slater, E. Prestat, A. Macedo, P. O'Brien, P. H. C. Camargo, S. J. Haigh, Real-time imaging and elemental mapping of AgAu nanoparticle transformations *Nanoscale* **2014**, *6*, 13598–13605.

[18] L. Russo, F. Merkoçi, J. Patarroyo, J. Piella, A. Merkoçi, N. G. Bastús, V. F. Puntes, Time- and Size-Resolved Plasmonic Evolution with nm Resolution of Galvanic Replacement Reaction in AuAg Nanoshells Synthesis *Submitt. Publ.*

[19] X. Xia, Y. Wang, A. Ruditskiy, Y. Xia, 25Th Anniversary Article: Galvanic Replacement: a Simple and Versatile Route To Hollow Nanostructures With Tunable and Well-Controlled Properties. *Adv. Mater.* **2013**, *25*, 6313–33.

[20] E. Gonzalez, J. Arbiol, V. F. Puntes, E. González, J. Arbiol, V. F. Puntes, Carving at the Nanoscale: Sequential Galvanic Exchange and Kirkendall Growth at Room Temperature *Science (80-.).* **2011**, *334*, 1377–1380.

[21] C. M. Cobley, Y. Xia, Engineering the properties of metal nanostructures via galvanic replacement reactions *Mater. Sci. Eng. R Reports* **2010**, *70*, 44–62.

[22] N. G. Bastús, F. Merkoçi, J. Piella, V. F. Puntes, Synthesis of Highly Monodisperse Citrate-Stabilized Silver Nanoparticles of up to 200 nm: Kinetic Control and Catalytic Properties *Chem. Mater.* **2014**, *26*, 2836–2846.

[23] H. S. Toh, C. Batchelor-McAuley, K. Tschulik, R. G. Compton, Electrochemical detection of chloride levels in sweat using silver nanoparticles: a basis for the preliminary screening for cystic fibrosis *Analyst* **2013**, *138*, 4292.

[24] K. Tschulik, C. Batchelor-McAuley, H.-S. Toh, E. J. E. Stuart, R. G. Compton, Electrochemical studies of silver

nanoparticles: a guide for experimentalists and a perspective *Phys. Chem. Chem. Phys.* **2014**, *16*, 616–623.

[25] R. Liu, J. Guo, G. Ma, P. Jiang, D. Zhang, D. Li, L. Chen, Y. Guo, G. Ge, Alloyed Crystalline Au–Ag Hollow Nanostructures with High Chemical Stability and Catalytic Performance *ACS Appl. Mater. Interfaces* **2016**, *8*, 16833–16844.

[26] S. E. F. Kleijn, S. C. S. Lai, M. T. M. Koper, P. R. Unwin, Electrochemistry of Nanoparticles *Angew. Chemie Int. Ed.* **2014**, *53*, 3558–3586.

[27] S. J. Cloake, H. S. Toh, P. T. Lee, C. Salter, C. Johnston, R. G. Compton, Anodic stripping voltammetry of silver nanoparticles: Aggregation leads to incomplete stripping *ChemistryOpen* **2015**, *4*, 22–26.

[28] L. R. Holt, B. J. Plowman, N. P. Young, K. Tschulik, R. G. Compton, The Electrochemical Characterization of Single Core-Shell Nanoparticles *Angew. Chemie Int. Ed.* **2016**, *55*, 397–400.

[29] E. N. Saw, V. Grasmik, C. Rurainsky, M. Epple, K. Tschulik, Electrochemistry at single bimetallic nanoparticles – using nano impacts for sizing and compositional analysis of individual AgAu alloy nanoparticles *Faraday Discuss.* **2016**, *157*, 243–284.

[30] Z. Liu, L. Huang, L. Zhang, H. Ma, Y. Ding, Electrocatalytic oxidation of d-glucose at nanoporous Au and Au-Ag alloy electrodes in alkaline aqueous solutions *Electrochim. Acta* **2009**, *54*, 7286–7293.

[31] C. Xu, J. Su, X. Xu, P. Liu, H. Zhao, F. Tian, Y. Ding, Low temperature CO oxidation over unsupported nanoporous gold *J. Am. Chem. Soc.* **2007**, *129*, 42–43.

[32] E. Herrero, L. J. Buller, H. D. Abruña, Underpotential deposition at single crystal surfaces of Au, Pt, Ag and other materials *Chem. Rev.* **2001**, *101*, 1897–1930.

[33] L. B. Rogers, J. C. Krause, J. Griess, D. B. Ehrlinger, The electrodeposition behavior of traces of silver *J. Electrochem. Soc.* **1949**, *95*, 33–46.

[34] G. Lai, L. Wang, J. Wu, H. Ju, F. Yan, Electrochemical stripping analysis of nanogold label-induced silver deposition for ultrasensitive multiplexed detection of tumor markers *Anal. Chim. Acta* **2012**, *721*, 1–6.

[35] X. Chu, Z. F. Xiang, X. Fu, S. P. Wang, G. L. Shen, R. Q. Yu, Silver-enhanced colloidal gold metalloimmunoassay for Schistosoma japonicum antibody detection *J. Immunol. Methods* **2005**, *301*, 77–88.

[36] J. Zhang, Z. Xiong, Z. Chen, Ultrasensitive electrochemical microcystin-LR immunosensor using gold nanoparticle functional polypyrrole microsphere catalyzed silver deposition for signal amplification *Sensors Actuators, B Chem.* **2017**, *246*, 623–630.

[37] S. W. T. Price, J. M. R. J. D. Speed, L. Calvillo, P. Kannan, a E. Russell, Exploring the First Steps in Core – Shell Electrocatalyst Preparation : In Situ Characterization of Cu and Pd shells on Supported Au Nanoparticles **2011**, 19448–19458.

[38] P. Mulvaney, T. Linnert, A. Henglein, Surface chemistry of colloidal silver in aqueous solution: Observations on chemisorption and reactivity *J. Phys. Chem.* **1991**, *95*, 7843–7846.

[39] W. He, X. Wu, J. Liu, X. Hu, K. Zhang, S. Hou, W. Zhou, S. Xie, Design of AgM bimetallic alloy nanostructures (M = Au, Pd, Pt) with tunable morphology and peroxidase-like activity *Chem. Mater.* **2010**, *22*, 2988–2994.

[40] M. Tominaga, T. Shimazoe, M. Nagashima, H. Kusuda, A. Kubo, Y. Kuwahara, I. Taniguchi, Electrocatalytic oxidation of glucose at gold-silver alloy, silver and gold nanoparticles in an alkaline solution *J. Electroanal. Chem.* **2006**, *590*, 37–46.

[41] M. Scanlon, P. Peljo, M. a Mendez, E. a. Smirnov, H. Girault, Charging and Discharging at the Nanoscale: Fermi Level Equilibration of Metallic Nanoparticles *Chem. Sci.* **2015**, 2705–2720.

[42] E. Prodan, P. Nordlander, Plasmon hybridization in spherical nanoparticles *J. Chem. Phys.* **2004**, *120*, 5444–5454.

[43] M. A. Mahmoud, M. A. El-Sayed, Gold nanoframes: Very high surface plasmon fields and excellent near-infrared sensors *J. Am. Chem. Soc.* **2010**, *132*, 12704–12710.

Electronic Supplementary Material

Tunable electrochemistry of gold-silver alloy nanoshells.

Lorenzo Russo,[1,2] Victor Puntes[1,3,4] and Arben Merkoçi[1,4](✉)

[1] *First address, Department, University, Cit[1] Catalan Institute of Nanoscience and Nanotechnology (ICN2), CSIC and BIST, Campus UAB, Bellaterra, 08193 Barcelona, Spain*

[2] *Universitat Autònoma de Barcelona (UAB), Campus UAB, 08193, Bellaterra, Barcelona, Spain.*

[3] *Vall d'Hebron Institut de Recerca (VHIR), 08035, Barcelona.*

[4] *Institució Catalana de Recerca i Estudis Avançats (ICREA), P. Lluís Companys 23, 08010 Barcelona, Spain.*

Supporting information to DOI 10.1007/s12274-****-****-* (automatically inserted by the publisher)

Figure S1. Comparison of DPVs of AuAg NSs and Ag NPs in different buffers and capping agents. When AuAg NSs are measured in PB 10 mM pH 7.5 (*black curve*, "**AuAgNSs@PVP in PB**") no relevant anodic current is observed. In absence of chlorides in the matrix no Ag corrosion is possible and therefore no stripping detection can be carried out. The same measurement in PBS (*grey curve*, "**AuAgNSs@PVP**") instead causes the anodic stripping signal of Ag to appear at +0.80 V vs RHE. When PVP-coated Ag NPs are used (*blue curve*, "**AgNPs@PVP**") a relatively intense oxidation current is recorded at potentials compatible with the at $Ag^0 \rightarrow Ag^+$ oxidation. The slight positive potential shift in the $Ag^0 \rightarrow Ag^+$ oxidation peak for PVP-coated Ag NPs is a product of the strong polymer affinity for silver, which can affect the pseudo-reference Ag/AgCl electrode. No oxidation peak is found when sodium citrate-coated Ag NPs (*red curve*, "**AgNPs@SC**") are measured, since their colloidal stability is easily compromised in the saline buffer.

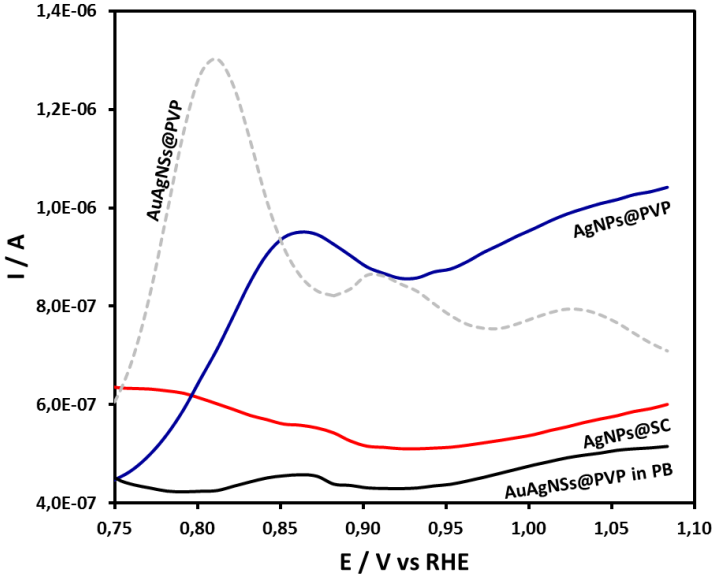

Address correspondence to Arben Merkoçi, email: arben.merkoci@icn2.cat